Quantitative observation of geotextile void network

Duhwan Kim
Senior Geotechnical Manager, Samsung C&T Coporation, Korea

David Frost
Professor, Georgia Institute of Technology, USA

ABSTRACT: The pore size of geotextiles and its distribution have been known to be significant parameters related to engineering properties. This paper presents results from a study undertaken to quantitatively evaluate microscopic void structure of a fibrous medium. An advanced image analysis technique was used to observe the evolution of the void microstructure from surfaces of coupons cut from epoxy impregnated specimens of a needle punched nonwoven geotextile. The voids enclosed by adjacent filaments were measured and expressed in terms of the local void ratio and the largest inscribing opening size. The load history of compression and interface shear of geotextiles against a textured geomembrane resulted in distinctive changes of micro-scale pore network.

Keywords: digital image analysis, geotextile, geomembrane, interface shear, pore, void

1 INTRODUCTION

Void networks and localized variation of void size have been useful means for evaluating material properties as well as predicting failure modes in various engineering fields. Clogging and filtration effects are known to be critical issues in geotextile applications (e.g., Prapaharan et al., 1989; Rebenfeld and Miller, 1995). The structures of materials made from non-woven filaments have been quantified by mechanical testing methods including sieve analysis (Rigo et al. 1990), mercury intrusion porosimetry (Bhatia and Smith, 1994), and in-plane water flow (Rebenfeld and Miller, 1995). Due to the disturbance of the delicate filament microstructure and the imposed boundary conditions, each method is known to provide significantly different results for the same geotextile (Bhatia et al., 1996). An advanced sample preparation method involving a low-viscosity epoxy resin and subsequent image analysis enabled the internal structure of the filaments in the geotextile microstructure to be observed.

2 EXPERIMENTAL PROGRAM AND DIGITAL IMAGE ANALYSIS

2.1 *Materials used*

Laboratory model testing was conducted using a needle punched nonwoven geotextile in combination with a smooth and a textured HDPE geomembrane that are widely used in practice. The selected geotextile is a polypropylene staple fabric. The geotextile has mass per unit area of $270\,g/m^2$, and tensile strength of 955 N based on the manufacturers literature. The geomembranes have nominal thickness is $1.5\,mm$, and yield tensile strength of 16 Pa. The surface textures of the geomembranes were formed through a coextruding process, which involved the rupture of bubbles formed by the rapid cooling of the blowing agent added inside the molten resin (Hebeler et al., 2005).

2.2 *Sample preparation*

A new experimental device and method were designed and developed to allow the geotextile to strain during interface shear against geomembranes. An epoxy impregnation method was adopted to encapsulate geotextiles compressed and/or sheared against geomembrane surfaces. At each desired stage, low-viscosity epoxy resin was impregnated into the specimen using air pressure of up to 8 kPa and allowed to cure for 12 hours at ambient room temperature (Kim and Frost, 2005; Kim, 2006; Kim and Frost, 2007).

After curing, the specimens were dissected to expose three orthogonal viewing planes, including the shear-direction, the cross-shear direction, and horizontal surfaces parallel to the geomembrane surface. Phases of the geotextile filaments and geomembranes surfaces were detected and measured through a sequence of image processing functions (Kim, 2006).

3 QUANTITATIVE OBSERVATION OF GEOTEXTILE PORE NETWORKS

3.1 *Concept of local void ratio*

Local void ratio is a dimensionless descriptor that is used to quantify the microscale distribution of pores in a material. This concept was first proposed by Oda in 1972 to evaluate the frequency distribution of voids in a sand specimen from 2-D images. This descriptor requires the generation of polygon elements enclosed by straight lines, which connect the centers of gravity of the solid phases. The local void ratio is then calculated from the ratio of the void area to the total solid area enclosed by each polygon (Figure 1). Bhatia and Soliman (1990) noted that the calculated mean value of the void ratio (e_{mean}) in Equation (1) is not equal to the global void ratio (e_s) as defined in Equation (2) unless all polygon sizes are equal.

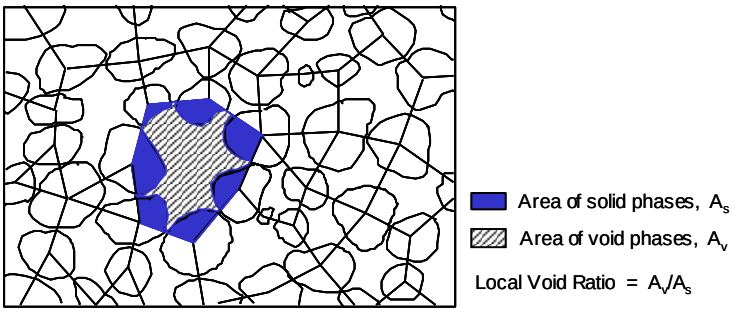

Figure 1. Local Void Ratio Measurement (After Oda, 1976).

$$e_{mean} = \frac{1}{k}(e_1 + e_2 + ... + e_k) = \frac{1}{k}(\frac{A_{v1}}{A_{s1}} + \frac{A_{v2}}{A_{s2}} + ... + \frac{A_{vk}}{A_{sk}}) \quad (1)$$

Where, k is the number of polygons

$$e_s = \frac{\text{Total area of voids in an image}}{\text{Total area of solids in an image}} = \frac{A_{v1} + A_{v2} + ... + A_{vk}}{A_{s1} + A_{s2} + ... + A_{sk}} = \frac{A_v}{A_s} \quad (2)$$

In order to overcome this problem, Frost and Kuo (1996) noted that the local void ratios weighted by the solid area (A_{si}) in each polygon would be more meaningful.

$$e_w = \frac{1}{\sum_{i=1}^{k} A_{si}}(\sum_{i=1}^{k} A_{si} \cdot e_i) \quad (3)$$

Substituting $e_i = \frac{A_{vi}}{A_{si}}$ into Equation (3) yields

$$e_w = \frac{A_v}{A_s} = e_s \tag{4}$$

Finally, the mean value of the local void ratio weighted with solid area becomes equal to the general void ratio of the image. Detailed information about the unbiased calculation of local void ratio and its distribution are found in Park (1999).

The algorithm developed by Frost and Kuo (1996) was applied to automatically calculate the unbiased local void ratio distribution (LVRD) independent of operator judgment.

3.2 *Concept of largest inscribing opening size*

Lombard et al. (1989) proposed a theoretical method to calculate the opening size of a heat bonded nonwoven geotextile. The method was based on the Poisson polyhedron theory (Matheron, 1971) and the results obtained using this method are known to yield results comparable to that of mechanical sieve analysis using glass beads (Rigo et al., 1990). In this study, the pore networks of geotextiles were quantified in terms of the largest inscribing opening size distribution (LIOS) from the 2-D images of representative specimen surfaces. The analysis was conducted using an automatic image analysis routine and compared with the theoretical estimates.

3.3 *Parametric studies on void networks descriptions of void ratio and LIOS*

Spatial array or distribution of micro-phases is often expressed as a lattice structure. The image analysis technique used in this study is based on measurement from two-dimensional images with aid of quantitative stereology which enables the collecting of three-dimensional information with limited errors (Underwood, 1969; Underwood, 1970, Gokhale and Drury, 1994). The relationship between various descriptors are discussed below using two basic formations of simple cubic (SC) and face-centered cubic (FCC) lattices subjected to various strain conditions.

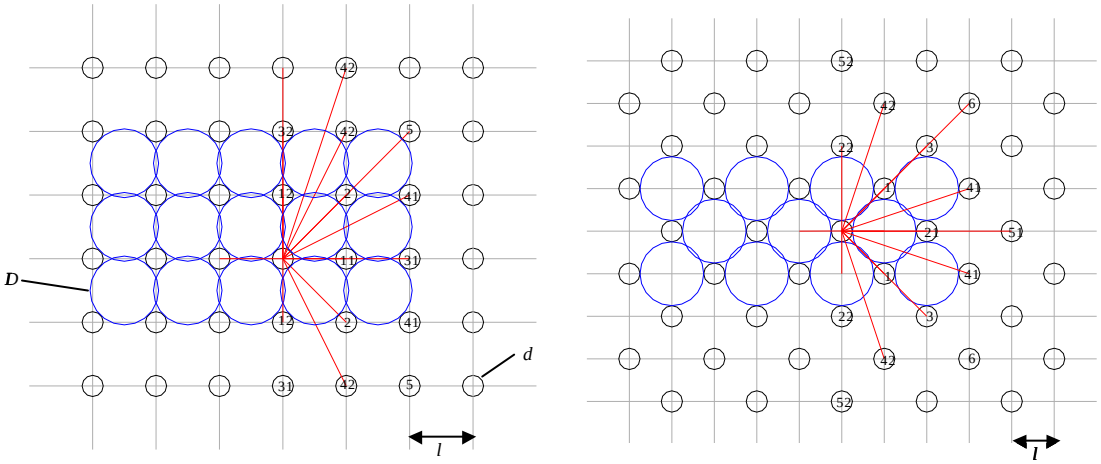

(a) (b)

Figure 2. Model of 2-D Lattice with measurements: (a) Simple Cubic; (b) Face Centered Cubic.

Schematic diagrams of two ideal lattices are illustrated in Figure 2, where each of the parameters is constant though the lattice regions. The solid and void parts are noted as α and β phases, respectively. Largest opening diameters inscribed by α phases can be calculated from the geometry of the adjacent four solid phases in these cases. It is noted that for a SC lattice, the enclosed opening diameter or LIOS is the same as the net distance to the nearest neighbor phase. However, the actual value varies with the distribution of phases and becomes different from the ideal lattice cases. Table 1 gives a summary of the parameters to be determined where, l is lattice distance, d is filament diameter, and k is ratio of the two values, l/d. One of merits of using LIOS is that this descriptor gives a direct measurement of the local void sizes.

Table 1. Calculation of Parameters of SC and FCC Lattices.

Parameter	Simple Cubic	Face Center Cubic
Void Ratio	$e_l = 4/\pi \cdot k^2 - 1$	$e_l = 8/\mu \cdot k^2 - 1$
LIOS	$D = (k\sqrt{2} - 1) \cdot d$	$D = (2k - 1) \cdot d$

It has a disadvantage that the measurement can be ambiguous if the void portion is relatively high and the solid phases have a small aspect ratio. In such cases, appropriate judgment is required to verify the adequate assignment of the center of the inscribing openings. The variation in parameters can be further expressed with regard to the changes of solid size, and strain types of the lattices including 2-D isotropic growing or shrinkage, 1-D stretch, and 2-D anisotropic straining with Poisson's ratio, ν.
Variations of LVRD in ideal SC and FCC lattices with various types of strain are illustrated in Figure 3, where, the initial solid diameter, center-to-center distance, and Poisson's ratio are set as 50, 100, and 0.2, respectively. The SC and FCC lattices show nonlinear relationships for the given conditions. Similarly, Figure 4 illustrates the change of LIOS with variation of filament size and lattice strain. The effects of filament diameter change are the same for SC and FCC lattices and the other parameters give different rates of inscribing diameter change with the increase of lattice distances. The change of LIOS with various deformation patterns of lattices is summarized in Table 2. The study with the lattice structures can be used as a reference to characterize the distribution pattern of void/filaments such as uniformity or randomness.

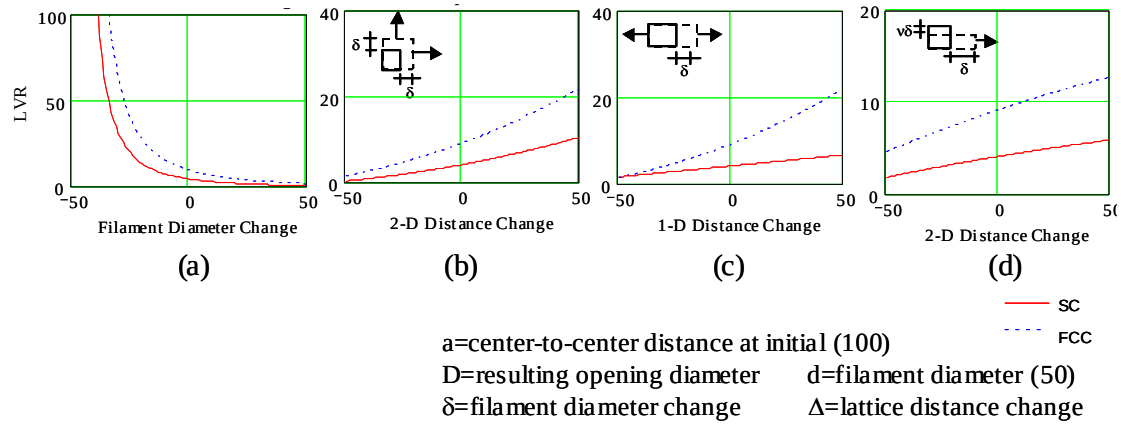

Figure 3. Variation of LVRD in SC and FCC Lattices with Change of Different Parameters: (a) Filament Diameter; (b) 2-D Isotropic Deformation; (c) 1-D Deformation; (d) Anisotropic Deformation with Poisson′s Ratio.

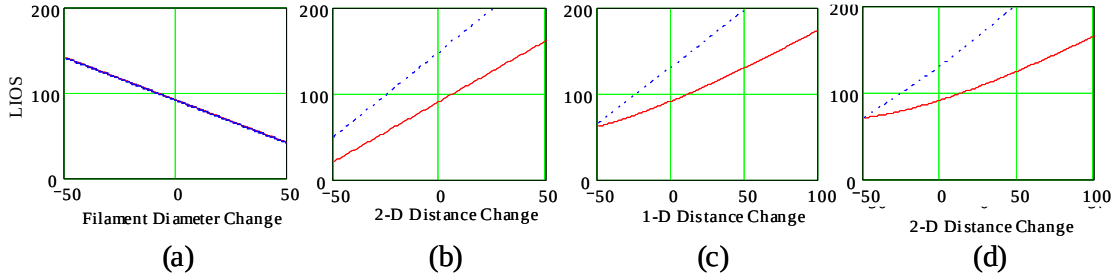

Figure 4. Variation of LIOS in SC and FCC Lattices with the Changes of Different Parameters: (a) Filament Diameter; (b) 2-D Isotropic Deformation; (c) 1-D Deformation; (d) Anisotropic Deformation with Poisson′s Ratio.

Table 2. Change of LIOS with Various Deformation Patterns of Lattices.

Variation	Simple Cubic	Face Center Cubic
Filament Diameter Decrease	$\sqrt{2}l - d - \delta$	$\sqrt{2}l - d - \delta$
2-D Isotropic Strain	$\sqrt{2}(l + \Delta) - d$	$2(l + \Delta) - d$
1-D Strain	$\sqrt{l^2 + (l + \Delta)^2} - d$	$2 \cdot l - d$
Anisotropic Strain with Poisson's ratio, ν	$\sqrt{(l + \Delta)^2 + (l - \nu \cdot \Delta)^2} - d$	$\frac{4}{l} \cdot \sec\left(\frac{\pi}{2} - 2 \cdot l \cdot \tan\left[\frac{l}{2(l + \Delta)}\right]\right)$

However, it is obvious that the LVRD and LIOS are determined by various factors and actual changes in the geotextiles can be quite different from the ideal cases due to complexity of deformation, reorientation and rearrangement of filaments, abrasion of material at the interface, amongst other factors.

4 SPATIAL DISTRIBUTION OF LOCAL VOID RATIO

4.1 *Evolution of local void ratio distribution*

Figure 5 illustrates typical distributions of incremental and cumulative local void ratio measurements of geotextile specimens sheared against textured geomembranes at two different normal stresses. The cross-shear surface under the same load conditions show increased number of small LVR. About 80% of the local void ratios are smaller than 6 and 3 at 100 kPa and 300 kPa, respectively (Figure 5c and 5d). The relatively low density of filaments in the shear surfaces is attributed to the geotextile strain and filament reorientation and/or rearrangement into the shear direction.

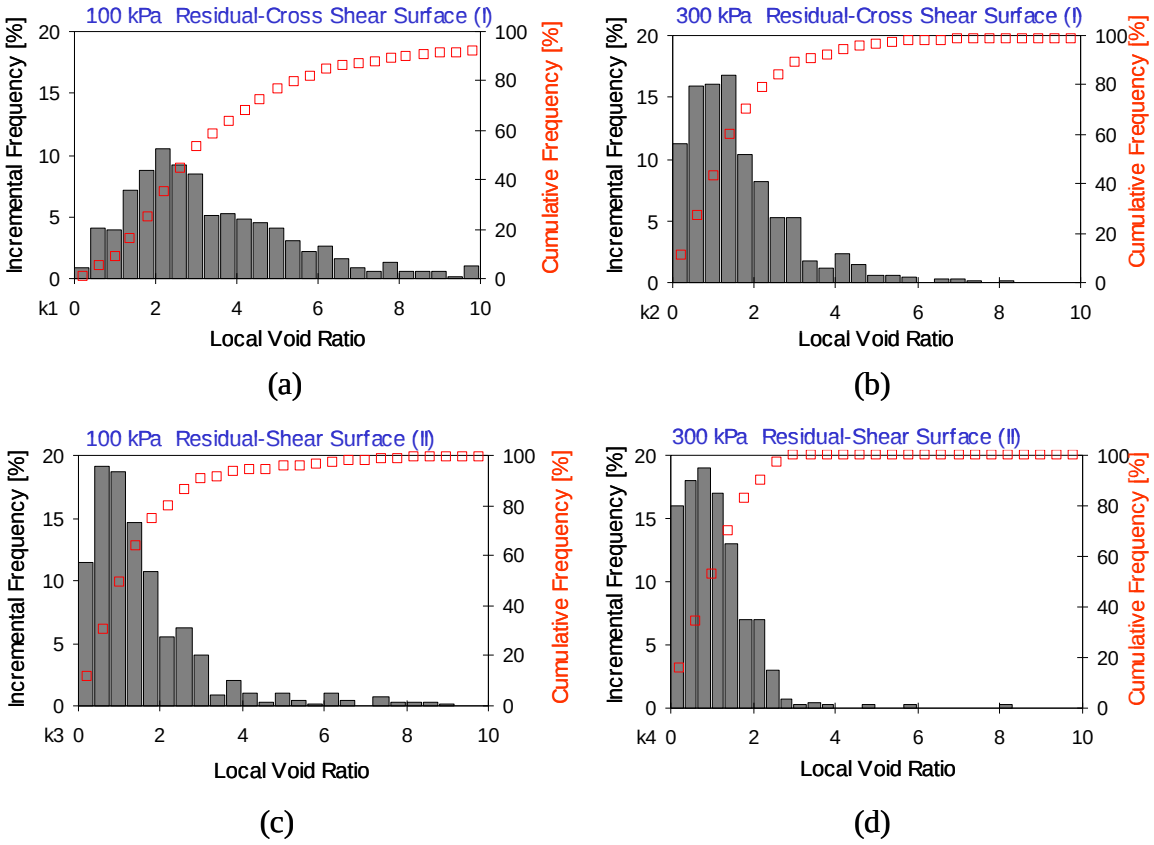

Figure 5. Local Void Ratio Measurement at Shear States: (a) Residual Shear at 100 kPa (Shear Surface); (b) Residual Shear at 300 kPa (Shear Surface); (c) Residual Shear at 100 kPa (Cross Shear Surface); (d) Residual Shear at 100 kPa (Cross Shear Surface).

Entropy indicates a measure of disorder in a discrete probability. This term can be calculated by appropriately modeling the distribution eliminating any bin having 0 probability. The entropy is 1 for distributions having the same probability for each bin and 0 if all data are in a single bin (Park, 1999).

The entropy values calculated from gamma and lognormal distribution models are shown in Figures 6a and 6b, respectively. The entropy values ranged from about 0.42 to 0.79 for mean local void ratios of 0.6 to 2.7 with only a minor difference between the two distribution models. The data shows the higher uniformity of the local void ratios at low normal stress and decreased uniformity for values of mean void ratio smaller than 1.0 due to compression and/or shear.

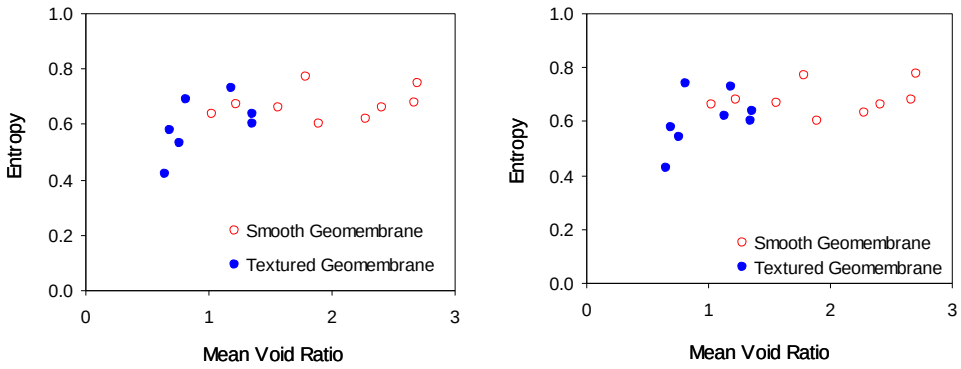

Figure 6. Variation of Entropy Value with Average Local Void Ratio: (a) Gamma Distribution; (b) Lognormal Distribution

4.2 *Evolution of geotextile void size*

Figure 7 presents the results for horizontal surfaces within the geotextile at different elevations. Figure 7a shows the effect of normal stress on the pore size distribution at mid-height within the specimen compressed against a smooth geomembrane surface. The cumulative distribution of voids smaller than 50 μm increased by about 25% as the normal stress increased from 100 to 300 kPa. It is noted that the horizontal sections parallel to the geotextile-geomembrane interface consisting of filament phases with large aspect ratios resulted in a higher population of small void areas. For example, the geotextile on a smooth surface in vertical section has a cumulative frequency of 26 % for pore diameters smaller than 50 μm at a normal stress of 100 kPa while the horizontal surface near the middle of the specimen (Figure 7a) has a corresponding value of 49% at the same normal stress. Figure 7b shows the variation of opening sizes on horizontal surfaces of the same specimen at different elevations. The data were collected from geotextile sections sheared against a textured geomembrane. It shows that the geotextile filaments are concentrated near the geomembrane texture features resulting in a high density of small openings at greater distances above the geomembrane-geotextile interface.

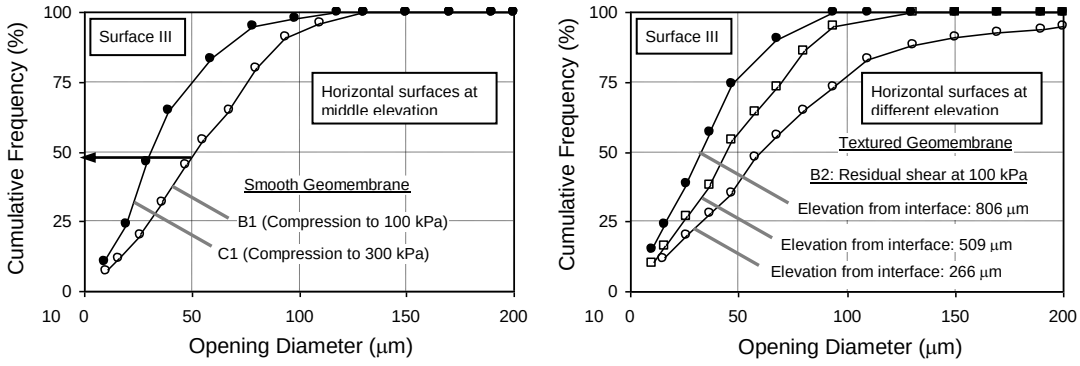

Figure 7. Results of LIOS measurements from horizontal surfaces: (a) effects of normal stress on a smooth geomembrane surface (middle elevation); (b) variation of LIOS at 100 kPa with elevation.

The responses of geotextile opening size distribution to compression or residual shear against smooth or textured geomembrane surfaces are further studied through a series of statistical analyses. Among the various curve fitting models, the beta distribution function was found as the best fitting curve by Pearson's space method and least square error method. The comparison of the measured cumulative frequency of pore size with the beta curve fitting results are presented in Figure 8 for the geotextile specimens placed on a textured geomembrane.

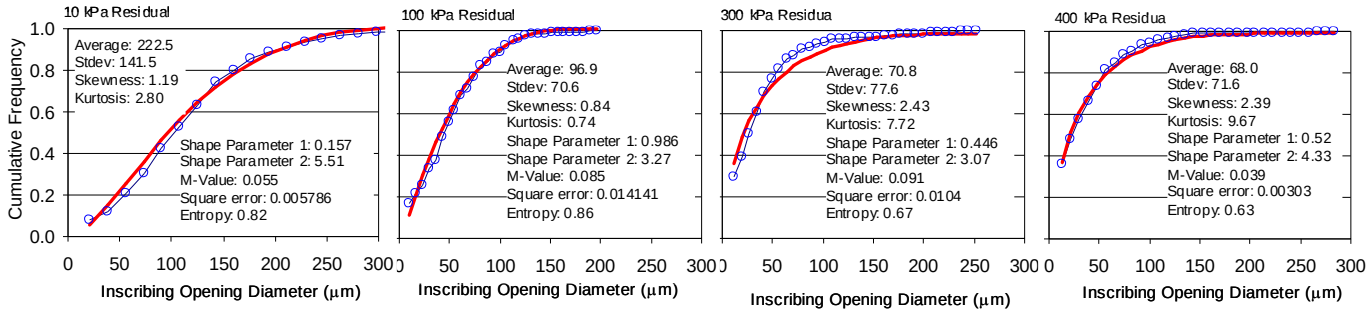

Figure 8. Largest Inscribing Opening Size Distribution and Beta Distribution Model-NPNW Geotextile on a Textured Geomembrane at Shear Surface

The filaments on the smooth geomembrane showed a linear relationship on the Pearson's probability distribution space while the textured specimens resulted in variations s with a large range. It is found that the LIOS data are mostly distributed in the regions of beta distribution of Pearson's probability distribution. The high normal stress and residual shear resulted in relatively low entropy of the opening size distribution (Figure 9). The relatively high values of entropy with mean opening size larger than 100 μm are for the cases in which hook and loop effect at low normal stress level of 10 kPa results in dilation of specimen and geotextile filament disturbance near the geomembrane-geotextile interface.

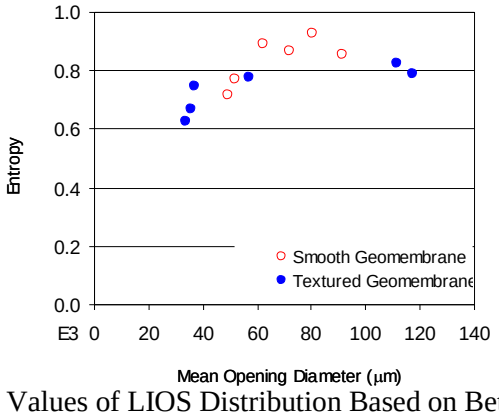

Figure 9. Entropy Values of LIOS Distribution Based on Beta Distribution Model.

5 CONCLUSIONS

Using image analysis and stereological investigation techniques, the pore structure of a needle-punched nonwoven geotextile was quantified. The load history such as compression or interface shear against a textured geomembrane resulted in distinctive differences in the micro-scale pore network. Local void ratio was found as a useful descriptor to quantitatively estimate void evolution of fibrous materials using advanced image analysis technique. This dimensionless descriptor can be used as a parameter to explain concentration of geotextile filament near geomembrane surface texture. LIOS has an advantage that it provides the actual scale of the pore size. LIOS was particularly useful for quantifying the horizontal surfaces of the geotextile specimen at different depths, where the networks consist of long curved features.

REFERENCES

Bhatia, S. K., & Soliman, A.F. 1990. Frequency Distribution of Void Ratio of Granular Materials Determined by an Image Analyzer, Journal of Soils and Foundations, Vol. 30(1), pp. 1-16.

Bhatia, S. K., Smith, J.L., & Christopher, B.R. 1996. Geotextile Characterization and Pore Size Distribution: Part III. Comparison of Methods and Application to Design, Geosynthetics International, Vol. 3 (3), pp. 301-328.

Frost, J. D. & Kuo, C.Y. 1996. Automated Determination of the Distribution of Local Void Ratio from Digital Images, Geotechnical Testing Journal, Vol. 19 (2), pp. 107-117.

Gokhale, A. M., & Drury, W.J. 1994. Efficient Measurement of Microstructural Surface Area Using Trisector, Metallurgical and Materials Transactions A, Vol. 25A, pp. 919-928.

Kim, D. 2006. Multi-Scale Assessment of Geotextile-Geomembrane Interaction, Ph.D. Thesis, School of Civil and Environmental Engineering, Georgia Institute of Technology, Atlanta, 276p.

Kim, D., & Frost, J.D. 2005. Multi-Scale Assessment of Geotextile-Geomembrane Interaction, NAGS 2005/GRI 19 Conference, Las Vegas, 8p.
Kim, D., & Frost, J.D. 2007. Investigation of filament distribution at geotextile/geomembrane interfaces, Journal of Geosynthetics International, Vol. 14, No.3, pp. 128-140.
Lombard, G., Rolin, A., & Wolff, C. 1989. Theoretical and Experimental Opening Sizes of Heat-Bonded Geotextiles, Textile Research Journal, Vol. 59(4), pp. 208-217.
Matheron, G. 1971. Les Polyedres Poissoniens Isotropes," Cahier interne du Centre de Morphologie Mathermatique, Fontainebleau., Vol., pp. 509-534.
Oda, M. 1972a. Initial Fabrics and Their Relations to Mechanical Properties of Granular Materials, Journal of Soils and Foundations, Vol. 12 (2), pp. 1-18.
Park, J. Y. 1999. A Critical Assessment of Moist Tamping and Its Effect on the Initial and Evolving Structure of Dilatant Triaxial Specimens, Ph.D. Thesis, School of Civil and Environmental Engineering, Georgia Institute of Technology, Atlanta, 384p.
Pearson, E. S. & Hartley, H.O. 1972. Biometrika Tables for Statistics, Cambridge University Press, London, 385p.
Prapaharan, S., Holtz, R.D., & Luna, J.D. 1989. Pore Size Distribution of Nonwoven Geotextiles, Geotechnical Testing Journal, GTJODJ, Vol. 12(4), pp. 261-268.
Rebenfeld, L. & Miller, B. 1995. Using Liquid Flow to Quantify the Pore Structure of Fibrous Materials, Journal of Textile Institute, Vol. 86(2), pp. 241-251.
Rigo, J. M., Lhote, F., Rollin, A.L., Mlynarek, J., & Lombard, G. 1990. Influence of Geotextile Structure on Pore Size Determination, ASTM Special Technical Publication, No. 1076, Vol., pp. 90-101.
Underwood, E.E. 1969. Stereology, or the Quantitative Evaluation of Microstructure, Journal of Microscopy, Vol. 89, Pt 2, pp. 161-180.
Underwood, E.E. 1970. Quantitative Stereology, Addison-Wesley Publishing Company, Inc., 274p.